Non-Linear Phase Different Control to Improve Dynamics of Bi-Articularly Actuated Manipulators

Valerio Salvucci and Takafumi Koseki
Department of Electrical Engineering and Information System The University of Tokyo
3-7-1 Hongo Bunkyoku Tokyo, Japan Email: valerio@koseki.t.u-tokyo.ac.jp, takafumikoseki@ieee.org

***Abstract*—There is a rising interest in bi-articular actuation for solving the known limitations of conventional robot arms. Actuator redundancy resulting from bi-articular actuation bring advantages such as increasing movement stability and efficiency in end effector force production. Actuator redundancy resolution is the first step in the control design for these robots, representing a key aspect for their performances. The Phase Different Control (PDC) resolves actuator redundancy on the basis of a linearized model derived from measured human muscle activity. Such linear model produces a non zero error in calculation between a desired output force and necessary inputs. In our previous work, the Non-Linear Phase Different Control (NLPDC) has been proposed to resolve actuator redundancy with no error under static conditions. In this work, NLPDC is implemented under dynamic conditions, and compared with PDC by simulating the dynamics a two-link planar arm. Performances such ad settling time and position error are highly improved when using NLPDC.**

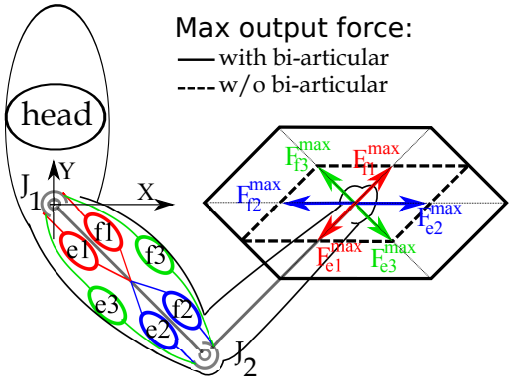

Fig. 1. Two-link arm with four mono- and two bi-articular actuators: model and resulting forces at the end effector

I. Introduction

Recently bi-articular actuation is rising in interest due to the numerous advantages it yields in robotic manipulation. Bi-articular actuators dramatically increase the range of end effector impedance which can be achieved without feedback [1], increasing the capability of path tracking and disturbance rejection using feedforward control [2], [3], and improving balance control for legged robots without force sensors [4]. Maximum output force at the end effector results in a more homogeneous distributed way when bi-articular actuators are present [5]. Bi-articular actuators transfer mechanical energy from proximal to distal joints [6]. This is a key aspect in legged robots for hopping [7], for jumping [8], and for running [9], In addition, multi-articular actuators, such as tri-articular actuators, increase efficiency in output force generation, as for example in lancelet-like swimming robots [10].

Bi-articularly actuated robots often present more actuators than joints, resulting in actuator redundancy. Actuator redundancy resolution is the first step in the control design for these robots strongly characterizing performances such as force precision and maximum magnitude [11]. A biologically inspired approach used to resolve actuator redundancy in a wide range of robot applications [10], [12], [13] is the Phase Different Control (PDC) [14]. According to PDC, the relationship between the end effector force and the six muscle inputs is determined using a linear model based on muscle activation level patterns, resulting from electromyography activity observation of human arm muscles while applying forces at the end effector under isometric and maximal effort conditions [14]. PDC approach, due to its linearization, presents an error in the calculation process from desired end effector force to muscle activation level inputs [15], [16]. To overcome such issue Non-Linear Phase Different Control (NLPDC), which combines PDC and a geometrically based non-linear model, has been proposed [17]. In our previous work [17] NLPDC has been implemented to resolve the actuation redundancy under static conditions.

In this work, we implement NLPDC under dynamic conditions, and compare it PDC by simulating the dynamics of a two-link planar robot arm actuated by two bi- and four mono-articular actuators.

In Section II, modeling of bi-articularly actuated robot arms is described. In Section III, the actuator redundancy problem is illustrated, and in Section IV PDC and NLPDC are presented. In Section V, how to implement NLPDC under dynamic conditions and the simulation setup is described. In Section VI, the simulation results are analyzed. In Section VII, the advantages of NLPDC are summarized.

II. Modeling of Bi-Articularly Actuated Robot Arms

Animals present a complex musculo-skeletal structure based on two types of muscles: mono-articular muscles producing a torque about one joint, and multi-articular muscles spanning more joints. The simplified model of the animal musculo-skeletal system shown in Fig. 1 is widely used for robot arms design [10], [12], [14], [18], [19]. This model is based on six contractile actuators — extensors (e1, e2, and e3) and flexors (f1, f2, and f3) — coupled in three antagonistic pairs: e1–f1 and e2–f2 are pairs of mono-articular actuators producing torques about joints 1 and 2, respectively; e3–f3 is

978-1-4799-0224-8/13/$31.00 ©2013 IEEE

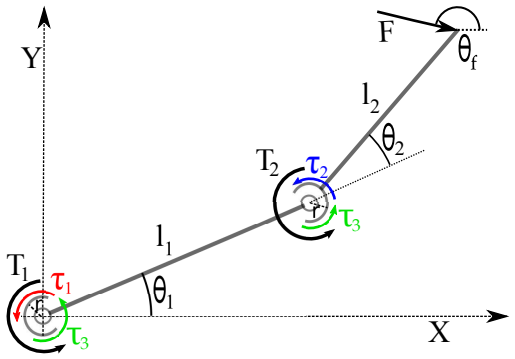

Fig. 2. Statics of two-link arm with four mono- and two bi-articular actuators

the pair of bi-articular actuators producing torque about joints 1 and 2 at the same time. Every of the six muscles has an activation level — e_1, e_2, e_3, f_1, f_2, f_3 — ranging from 0, which means no muscle contractile force produced, to 100% corresponding to the maximum muscle contractile force — e_1^{max}, e_2^{max}, e_3^{max}, f_1^{max}, f_2^{max}, f_3^{max}.

III. Actuator Redundancy Problem

A robot arm modeled as in Fig. 1 is redundant in actuation: has six actuators and two DOF. The resulting statics are shown in Fig. 2 where $\boldsymbol{F}$ is a general force at the end effector; T_1 and T_2 are total torques about joints 1 and 2, respectively; τ_1 and τ_2 are torques produced by mono-articular actuators about joints 1 and 2, respectively; τ_3 is the bi-articular torque produced about both joints simultaneously. The joint torques $\boldsymbol{T}$ are:

$$\boldsymbol{T} = \begin{bmatrix} T_1 \\ T_2 \end{bmatrix} = \begin{bmatrix} 1 & 0 & 1 \\ 0 & 1 & 1 \end{bmatrix} \begin{bmatrix} \tau_1 \\ \tau_3 \\ \tau_3 \end{bmatrix} = \begin{bmatrix} \tau_1 + \tau_3 \\ \tau_2 + \tau_3 \end{bmatrix} \tag{1}$$

The problem represented by (1) is referred in the following as the redundancy actuator problem. Given $\boldsymbol{\tau} = [\tau_1, \tau_2, \tau_3]^T$, it is possible to determine $\boldsymbol{T}$ by using (1), and $\boldsymbol{F}$ by:

$$\boldsymbol{F} = \left(J^T\right)^{-1} \boldsymbol{T} \tag{2}$$

where

$$J = \begin{bmatrix} -l_1\sin(\theta_1) - l_2\sin(\theta_1+\theta_2) & -l_2\sin(\theta_1+\theta_2) \\ l_1\cos(\theta_1) + l_2\cos(\theta_1+\theta_2) & l_2\cos(\theta_1+\theta_2) \end{bmatrix} = \begin{bmatrix} a & b \\ c & d \end{bmatrix} \tag{3}$$

On the other hand, given $\boldsymbol{F}$, and therefore $\boldsymbol{T}$, it is generally not possible to determine uniquely $\boldsymbol{\tau}$ due to the presence of bi-articular actuators (see (1)).

For both PDC and NLPDC approaches the three joint actuator torques $\boldsymbol{\tau}$ are functions of the six muscle forces. They are widely modeled in static conditions as [14]:

$$\boldsymbol{\tau} = \begin{bmatrix} (f_1 - e_1)r - Kr^2(f_1 + e_1)\Delta\theta_1 \\ (f_2 - e_2)r - Kr^2(f_2 + e_2)\Delta\theta_2 \\ (f_3 - e_3)r - Kr^2(f_3 + e_3)(\Delta\theta_1 + \Delta\theta_2) \end{bmatrix} \tag{4}$$

where r is distance between the joint and the point where the muscle force is applied, considered to be the same for all the muscles; K is a elastic constant considered to be independent from joint angles ($\boldsymbol{\theta}$), and the same for all muscles; $\Delta\boldsymbol{\theta}$ is the difference between the actual position and the muscle natural length position. In the following, $\Delta\boldsymbol{\theta}$ is considered to be null, that is the actuators are always at natural length, therefore:

$$\boldsymbol{\tau} = \begin{bmatrix} (f_1 - e_1)r \\ (f_2 - e_2)r \\ (f_3 - e_3)r \end{bmatrix} \tag{5}$$

Hence the statics of the arm in Fig. 1 are:

$$\boldsymbol{T} = \begin{bmatrix} (f_1 - e_1)r + (f_3 - e_3)r \\ (f_2 - e_2)r + (f_3 - e_3)r \end{bmatrix} \tag{6}$$

IV. Actuator Redundancy Resolution Methods

A. PDC

The muscle activation level patterns on which PDC is based are shown in Fig. 3(a). These patterns are the linearization of the patterns resulting from electromyography activity observation of human arm muscles while applying forces at the end effector under isometric and maximal effort conditions [14]. The six muscle activation level patterns are expressed in respect to the force direction θ_f. According to

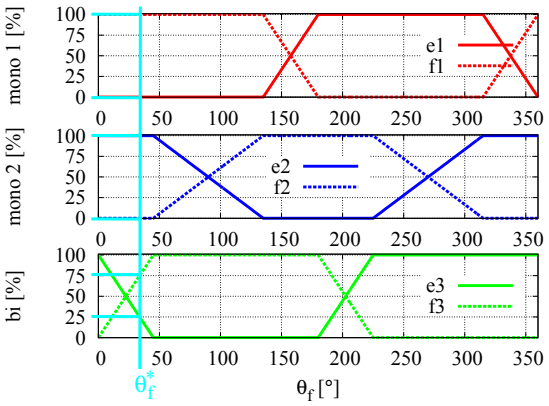

(a) Muscle activation level patterns used as input references for PDC approach

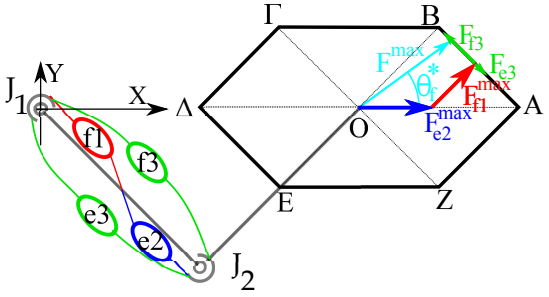

(b) Resulting end effector maximum force

Fig. 3. PDC approach, muscle activation level patterns and resulting end effector maximum force [14]

PDC approach, the end effector maximum force $\boldsymbol{F}^{max}$ with angle θ_f^* in Fig. 3(b) is obtained using the muscle activation level patterns in Fig. 3(a) as inputs. $\boldsymbol{F}^{max}$ in direction θ_f^* is the sum of the six forces produced by the six muscles:

$$\boldsymbol{F}^{max} = \boldsymbol{F}_{e1} + \boldsymbol{F}_{f1} + \boldsymbol{F}_{e2} + \boldsymbol{F}_{f2} + \boldsymbol{F}_{e3} + \boldsymbol{F}_{f3} \tag{7}$$

For the particular case in Fig. 3(b), where $l_1 = l_2 = 1$ m, $\theta_1 = -45°$, $\theta_2 = 90°$, $e_i^{max} r = f_i^{max} r = 1$ Nm for $i = (1,2,3)$, and $\theta_f^* = 33.75°$ results:

$$\boldsymbol{F}^{max} = \boldsymbol{F}_{f1}^{max} + \boldsymbol{F}_{e2}^{max} + 0.25\boldsymbol{F}_{e3}^{max} + 0.75\boldsymbol{F}_{f3}^{max} \tag{8}$$

The six muscle activation levels producing $\boldsymbol{F}^{max}$ in direction θ_f^* are calculated as follows:

1) On the basis of the Jacobian (3), the actual configuration (θ_1 and θ_2) and the maximum muscle forces, calculate the angles α, β, γ, δ, ε, and ζ, defined as the angles between the x-axis and the line passing through the center O and points A, B, Γ, Δ, E, and Z in Fig. 3(b), respectively.
2) Calculate the muscle activation level — e_1, e_2, e_3, f_1, f_2, f_3 — using the graph in Fig. 3(a). The graphical illustration of the muscle activation levels for PDC (Fig. 3(a)), is mathematically represented by a set of six piecewise linear functions, one for every muscle. Every piece wise function is defined on six intervals, as shown in Tab. I in the PDC rows.

The $\boldsymbol{\tau}$ producing $\boldsymbol{F}^{max}$ are calculated using (5). In the case illustrated in Fig. 3(b):

$$\boldsymbol{\tau} = \begin{bmatrix} (f_1 - e_1)r \\ (f_2 - e_2)r \\ (f_3 - e_3)r \end{bmatrix} = \begin{bmatrix} f_1^{max} r \\ -e_2^{max} r \\ \left(0.75 f_3^{max} - 0.25 e_3^{max}\right) r \end{bmatrix} \tag{9}$$

B. NLPDC

The muscle activation levels that produce $\boldsymbol{F}^{max}$ on direction θ_f^* using the proposed NLPDC approach are shown in Tab. I in the NLPDC rows. NLPDC is based on PDC as uses the same muscle activation levels when they are null (0) or maximum (e_i^{max} and f_i^{max} for $i = (1,2,3,)$). Elsewhere, the muscle activation levels are derived on the basis of the robot arm geometry (as shown in [17]), resulting in:

$$m_1^{\zeta\alpha} = \frac{(-e_2^{max} - e_3^{max})(a + c\tan(\theta_f^*))}{d\tan(\theta_f^*) + b} + e_3^{max} \tag{10}$$

$$m_3^{\alpha\beta} = \frac{(-f_1^{max} - e_2^{max})(a + c\tan(\theta_f^*))}{(d-c)\tan(\theta_f^*) + b - a} - f_1^{max} \tag{11}$$

$$m_2^{\beta\gamma} = \frac{(f_1^{max} + f_3^{max})(b + d\tan(\theta_f^*))}{c\tan(\theta_f^*) + a} - f_3^{max} \tag{12}$$

$$m_1^{\gamma\delta} = \frac{(f_2^{max} + f_3^{max})(a + c\tan(\theta_f^*))}{d\tan(\theta_f^*) + b} - f_3^{max} \tag{13}$$

$$m_3^{\delta\varepsilon} = \frac{(e_1^{max} + f_2^{max})(a + c\tan(\theta_f^*))}{(d-c)\tan(\theta_f^*) + b - a} + e_1^{max} \tag{14}$$

$$m_2^{\varepsilon\zeta} = \frac{(-e_1^{max} - e_3^{max})(b + d\tan(\theta_f^*))}{c\tan(\theta_f^*) + a} + e_3^{max} \tag{15}$$

where a, b, c, and d are the Jacobian matrix components as in (3); m_j^{kl} is the activation level of muscle m (where m is either e or f) that produce torque τ_j with $j = (1,2,3)$ such that the end effector force is maximum in direction θ_f^*. The calculated output force direction (θ_f) is equal to the desired output force direction (θ_f^*), if the two muscles that produce force in direction k and l have maximum activation level.

The values σ_1, σ_2, and σ_3 represent the minimum activation level between two muscles of every antagonistic pair. In this work, they are set to 0.

A graphical example of the use of NLPDC is illustrated in Fig. 4(b) for $l_1 = l_2 = 1$ m, $\theta_1 = -45°$, $\theta_2 = 90°$, $e_1^{max} r = f_1^{max} r = e_2^{max} r = f_2^{max} r = e_3^{max} r = f_3^{max} r = 1$ Nm, and $\sigma_1 = \sigma_2 = \sigma_3 = 0$. $\boldsymbol{F}^{max}$ for $\theta_f^* = 33.75°$ is:

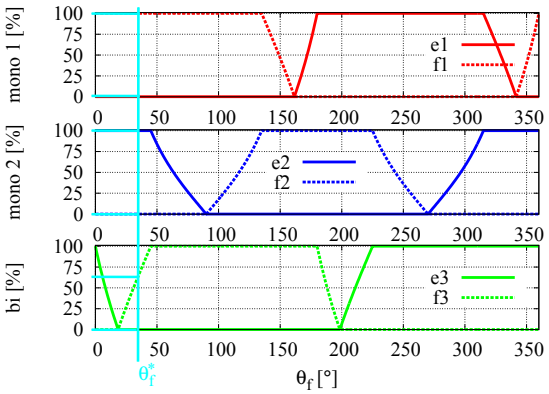

(a) Muscle activation level patterns

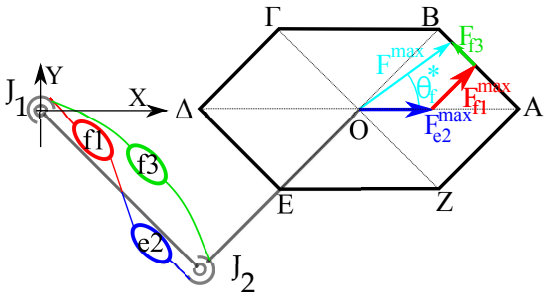

(b) End effector maximum force

Fig. 4. NLPDC approach: muscle activation level patterns and end effector maximum force

$$\boldsymbol{F}^{max} = \boldsymbol{F}_{f1}^{max} + \boldsymbol{F}_{e2}^{max} + 0.6\boldsymbol{F}_{f3}^{max} \tag{16}$$

Using Tab. I results:

$$\boldsymbol{\tau} = \begin{bmatrix} (f_1 - e_1)r \\ (f_2 - e_2)r \\ (f_3 - e_3)r \end{bmatrix} = \begin{bmatrix} (f_1^{max} - 0)r = f_1^{max} r \\ (0 - e_2^{max})r = -e_2^{max} r \\ \left(\left(m_3^{\alpha\beta}\right)^{+} - \left(m_3^{\alpha\beta}\right)^{-}\right) r = 0.6 f_3^{max} r \end{bmatrix} \tag{17}$$

V. Simulation Description and Analysis Method

The dynamics of a two-link planar robot arm actuated by two bi- and four mono-articular actuators are simulated. In Fig. 5 the robot arm and the coordinate frame are shown. The end effector initial position are x^{ini} and y^{ini}, while $\boldsymbol{X}^{des}$ is the desired position, defined as:

$$\boldsymbol{X}^{des} = \begin{bmatrix} x^{des} \\ y^{des} \end{bmatrix} = \begin{bmatrix} x^{ini} + dist\cos(\theta^{des}) \\ y^{ini} + dist\sin(\theta^{des}) \end{bmatrix}, \tag{18}$$

where $dist$ and θ^{des} are the desired end effector position magnitude and direction, respectively.

TABLE I. MUSCLE ACTIVATION LEVELS FOR PDC AND NLPDC. $(x)^+ = \max(0,x)$ AND $(x)^- = \max(-x,0)$

		$\zeta \le \theta_f^* < \alpha$	$\alpha \le \theta_f^* < \beta$	$\beta \le \theta_f^* < \gamma$	$\gamma \le \theta_f^* < \delta$	$\delta \le \theta_f^* < \varepsilon$	$\varepsilon \le \theta_f^* < \zeta$
e_1	PDC	$e_1^{max} - \frac{\theta_f^* - \zeta}{\alpha - \zeta} e_1^{max}$	0	0	$\frac{\theta_f^* - \gamma}{\delta - \gamma} e_1^{max}$	e_1^{max}	e_1^{max}
	NLPDC	$\left(m_1^{\zeta\alpha}\right)^- + \sigma_1$			$\left(m_1^{\gamma\delta}\right)^- + \sigma_1$		
f_1	PDC	$\frac{\theta_f^* - \zeta}{\alpha - \zeta} f_1^{max}$	f_1^{max}	f_1^{max}	$f_1^{max} - \frac{\theta_f^* - \gamma}{\delta - \gamma} f_1^{max}$	0	0
	NLPDC	$\left(m_1^{\zeta\alpha}\right)^+ + \sigma_1$			$\left(m_1^{\gamma\delta}\right)^+ + \sigma_1$		
e_2	PDC	e_2^{max}	e_2^{max}	$e_2^{max} - \frac{\theta_f^* - \beta}{\gamma - \beta} e_2^{max}$	0	0	$\frac{\theta_f^* - \varepsilon}{\zeta - \varepsilon} e_2^{max}$
	NLPDC			$\left(m_2^{\beta\gamma}\right)^- + \sigma_2$			$\left(m_2^{\varepsilon\zeta}\right)^- + \sigma_2$
f_2	PDC	0	0	$\frac{\theta_f^* - \beta}{\gamma - \beta} f_2^{max}$	f_2^{max}	f_2^{max}	$f_2^{max} - \frac{\theta_f^* - \varepsilon}{\zeta - \varepsilon} f_2^{max}$
	NLPDC			$\left(m_2^{\beta\gamma}\right)^+ + \sigma_2$			$\left(m_2^{\varepsilon\zeta}\right)^+ + \sigma_2$
e_3	PDC	e_3^{max}	$e_3^{max} - \frac{\theta_f^* - \alpha}{\beta - \alpha} e_3^{max}$	0	0	$\frac{\theta_f^* - \delta}{\varepsilon - \delta} e_3^{max}$	e_3^{max}
	NLPDC		$\left(m_3^{\alpha\beta}\right)^- + \sigma_3$			$\left(m_3^{\delta\varepsilon}\right)^- + \sigma_3$	
f_3	PDC	0	$\frac{\theta_f^* - \alpha}{\beta - \alpha} f_3^{max}$	f_3^{max}	f_3^{max}	$f_3^{max} - \frac{\theta_f^* - \delta}{\varepsilon - \delta} f_3^{max}$	0
	NLPDC		$\left(m_3^{\alpha\beta}\right)^+ + \sigma_3$			$\left(m_3^{\delta\varepsilon}\right)^+ + \sigma_3$	

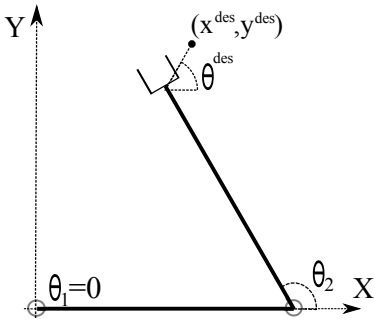

Fig. 5. Robot arm coordinate frame used in the simulation

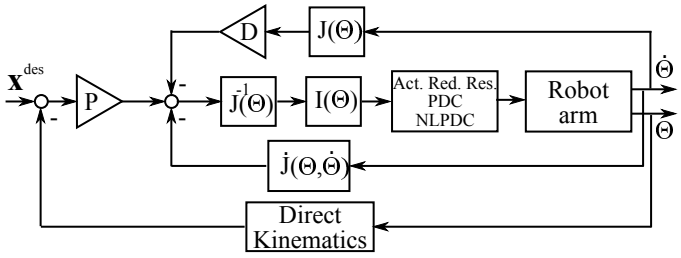

Fig. 6. Feedback position control with PD and compensation of robot arm inertia

A position feedback controller with compensation of the robot arm inertia is designed in the operational space as shown in Fig. 6, where $I(\boldsymbol{\theta})$ is the robot arm inertia matrix. The actuation redundancy is resolved by either PDC or NLPDC approach from the desired virtual force at the end effector as in the following.

The FB controlled determine a desired virtual force $\boldsymbol{F}^v$:

$$\boldsymbol{F}^v = \begin{bmatrix} P(x^{des} - x^{act}) - D\dot{x}^{act} \\ P(y^{des} - y^{act}) - D\dot{y}^{act} \end{bmatrix} \tag{19}$$

The direction of $\boldsymbol{F}^v$ (θ_f^v) is used to calculate the six actuator inputs (m_i^{max}, for $m = (e,f)$ and $i = (1,2,3)$) that produce a maximum output force $\boldsymbol{F}^{max}$ in direction θ_f^v, using either PDC or NLPDC as shown in Section IV. As the relationship between output force and actuator input torque is linear for a given robot arm configuration and output force direction, the six actuator inputs (m_i^{input}, for $m = (e,f)$ and $i = (1,2,3)$) are multiplied by the ratio between the magnitude of $\boldsymbol{F}^v$ and $\boldsymbol{F}^{max}$, resulting in:

$$m_i^{input} = \frac{|\boldsymbol{F}^v|}{|\boldsymbol{F}^{max}|} m_i^{max} \tag{20}$$

This is how both the PDC and NLPDC are implemented under dynamic conditions.

TABLE II. SIMULATION PARAMETERS

Parameter	value
Length link 1 and 2	1 m
Mass 1 and 2	5 Kg
COM 1 and 2	0.5 m
Momentum of Inertia 1 and 2	1.67 Kg/m^2
P and D gains	39.5, 8.9

The parameters used in the simulation are shown in Tab. II. P gain is designed so to have an end effector frequency response of 1 Hz to a position step input along $\theta^{des} = 45°$ with $dist = 0.01$ m when $\boldsymbol{\theta} = [0°, 90°]^T$. D gain is designed to have a damping factor of $\sqrt{2}$.

Simulation is performed varying θ^{des} from 0 to 360° in increments of 1°, while the desired distance is constant, $dist = 0.01$ m. The robot arm initial configuration is also varied: $\theta_1 = 0$, and θ_2 is varied from 15° to 165° in increments of 5°. The end effector desired position is given as a step input. The joint actuator torque is designed big enough not to saturate.

Four parameters are calculated in order to compare PDC and NLPDC approaches.

- Position error:

$$err(t) = \sqrt{(x^{des} - x(t))^2 + (y^{des} - y(t))^2} \tag{21}$$

- Settling time st: time elapsed from the application of the step input to the time at which $err(t)$ has entered and remained within a band of 2% of $dist$.

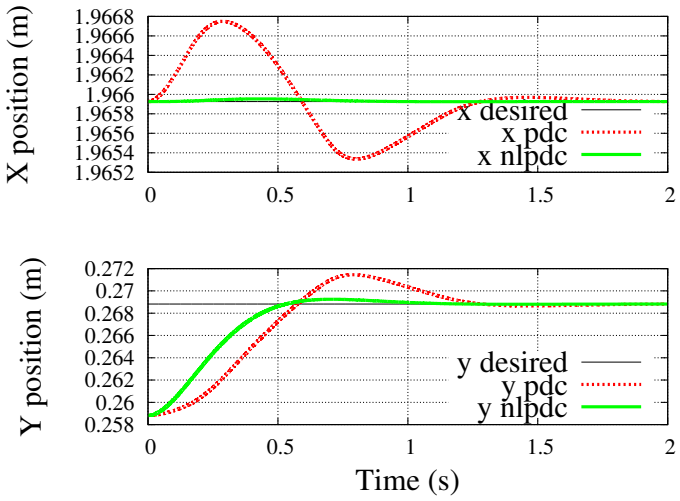

(a) End effector position

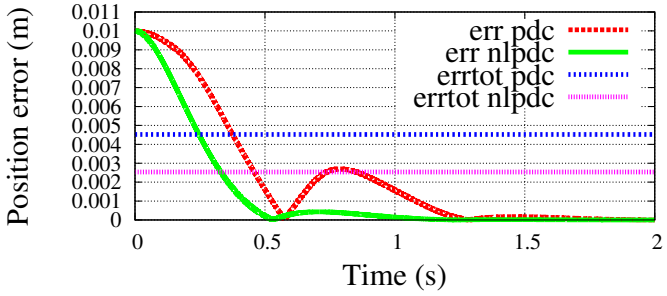

(b) Position error ($err(t)$) and total error for $\theta^{des} = 0°$ ($errtot_0$)

Fig. 7. Response of the end effector to a step input for PDC and NLPDC; $\theta_1 = 0$, $\theta_2 = 15°$, $dist = 0.01$, and $\theta^{des} = 90°$.

- Total position error, for a given desired output direction $\theta^{des} \in (0,360)°$:

$$errtot_{\theta^{des}} = \int_0^{st} err(t)\delta t \tag{22}$$

- Total error, for a given robot arm configuration (θ_1, θ_2):

$$errconf_{\theta_1,\theta_2} = \frac{1}{360} \sum_{\theta^{des}=0}^{359} errtot_{\theta^{des}} \tag{23}$$

VI. Results

In Fig. 7 PDC and NLPDC are compared taking into account the end effector position response to a step input. The robot arm configuration is $\theta_1 = 0$, $\theta_2 = 15°$, while desired direction $\theta^{des} = 90°$. End effector position, error ($err(t)$) and total error ($errtot_{90}$) are shown. When using PDC $st = 1.22$ s and $errtot_{90} = 0.0045$ s*m, which are greater than the NLPDC case, i.e. $st = 0.95$ s and $errtot_{90} = 0.0025$ s*m.

A comparison for the same arm configuration as in Fig. 7 (i.e. $\theta_1 = 0$, $\theta_2 = 15°$), while varying θ^{des} from 0 to 360° in increments of 1° is shown in Fig. 8. Settling time (st) and its maximum value (st^{max}), as well as total position error ($errtot_{\theta^{des}}$) and its average in the specific arm configuration

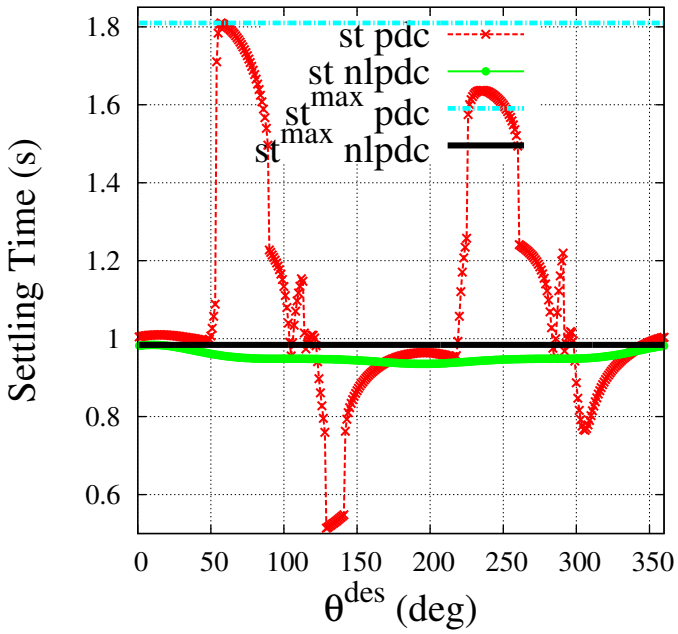

(a) Settling time (st) and its maximum (st^{max}).

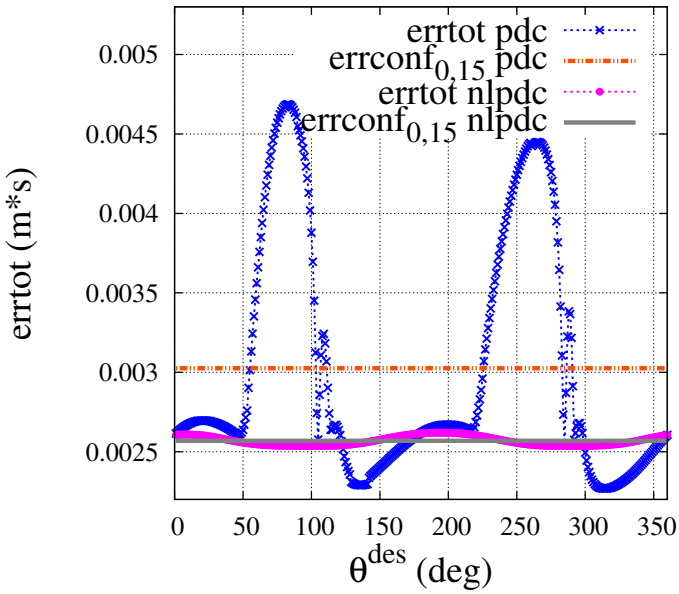

(b) Total position error ($errtot_{\theta^{des}}$) and its average ($errconf_{0,15}$).

Fig. 8. Comparing PDC and NLPDC for $\theta_1 = 0$, $\theta_2 = 15°$, and $\theta^{des} \in (0,360)°$.

($errconf_{0,15}$) are illustrated. It emerges that when using PDC, the maximum settling time (i.e. the worse response for a given arm configuration), as well the mean of the position error (representing an index of precision) are higher. In fact, for PDC $st^{max} = 1.81$ s and $errconf_{0,15} = 0.0030$ m*s, while for NLPDC $st^{max} = 0.98$ s and $errconf_{0,15} = 0.0025$ m*s. There are values of θ^{des} (for example around 140° and 310°) where the PDC shows a lower st and $errtot_{\theta^{des}}$. For such θ^{des} the error in the redundancy resolution of PDC plays in favour of

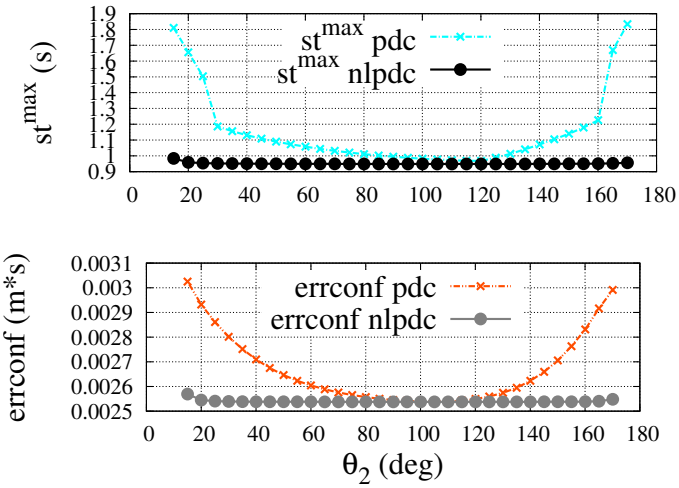

Fig. 9. Maximum settling time (st^{max}), and average of total position error ($errconf_{\theta_1,\theta_2}$) of PDC and NLPDC for $\theta_1 = 0°$, and $\theta_2 \in (15, 165)°$

the non linearity of the robot arm. However, such conditions are met for small ranges, and the advantage of PDC in respect to NLPDC is significantly smaller than the advantages of the NLPDC in other θ^{des} ranges, as is shown in the comparison carried out in the following.

In Fig. 9 PDC and NLPDC are compared in terms of maximum settling time (st^{max}), and average of total position error ($errconf_{\theta_1,\theta_2}$). These two parameters are calculated varying the robot arm initial configuration: $\theta_1 = 0$, while θ_2 is varied from 15° to 165° in increments of 5°. From Fig. 9 it is deduced that st^{max} and $errconf_{\theta_1,\theta_2}$ are smaller for the NLPDC approach in all the workspace. The advantages of NLPDC increase when the manipulator moves towards singular configurations, i.e. θ_2 approaches 0 or 180°. This is in concordance with the error profiles shown by PDC in static conditions [20].

VII. CONCLUSIONS

The Non-Linear Phase Different Control (NLPDC) approach to resolve actuators redundancy for bi-articularly actuated robot arms is implemented under dynamic conditions. A comparison with the Phase Different Control (PDC) is carried out by simulation means.

In respect to PDC, NLPDC achieves better performance:

1) Reducing settling time
2) Reducing position error

In addition, it is shown how the magnitude of such improvements vary with the robot arm configuration. The reduction in both settling time and position error increases when the arm approaches singular configurations, as for example when the robot arm stretches. Fast and precise control in such configuration is fundamental for stable jumping and walking actions in robotic applications.

REFERENCES

[1] N. Hogan, "Impedance control: An approach to manipulation: Part III—Applications," *Journal of Dynamic Systems, Measurement, and Control*, vol. 107, no. 1, pp. 17–24, Mar. 1985.

[2] T. Horita, P. V. Komi, C. Nicol, and H. Kyrlinen, "Interaction between pre-landing activities and stiffness regulation of the knee joint musculoskeletal system in the drop jump: implications to performance," *European Journal of Applied Physiology*, vol. 88, no. 1-2, pp. 76–84, Nov. 2002, PMID: 12436273.

[3] K. Yoshida, T. Uchida, and Y. Hori, "Novel FF control algorithm of robot arm based on bi-articular muscle principle - emulation of muscular viscoelasticity for disturbance suppression and path tracking," in *Industrial Electronics Society, 2007. IECON 2007. 33rd Annual Conference of the IEEE*, 2007, pp. 310–315.

[4] S. Oh, Y. Kimura, and Y. Hori, "Reaction force control of robot manipulator based on biarticular muscle viscoelasticity control," in *Advanced Intelligent Mechatronics (AIM), 2010 IEEE/ASME International Conference on*, 2010, pp. 1105–1110.

[5] T. Fujikawa, T. Oshima, M. Kumamoto, and N. Yokoi, "Output force at the endpoint in human upper extremities and coordinating activities of each antagonistic pairs of muscles." *Transactions of the Japan Society of Mechanical Engineers. C*, vol. 65, no. 632, pp. 1557–1564, 1999.

[6] G. J. Van Ingen Schenau, "From rotation to translation: Constraints on multi-joint movements and the unique action of bi-articular muscles," *Human Movement Science*, vol. 8, no. 4, pp. 301–337, Aug. 1989.

[7] M. A. Lewis, M. R. Bunting, B. Salemi, and H. Hoffmann, "Toward ultra high speed locomotors: Design and test of a cheetah robot hind limb," in *IEEE International Conference on Robotics and Automation (ICRA)*, 2011.

[8] T. Oshima, N. Momose, K. Koyanagi, T. Matsuno, and T. Fujikawa, "Jumping mechanism imitating vertebrate by the mechanical function of bi-articular muscle," in *Mechatronics and Automation, 2007. ICMA 2007. International Conference on*, 2007, pp. 1920–1925.

[9] R. Niiyama, S. Nishikawa, and Y. Kuniyoshi, "Athlete robot with applied human muscle activation patterns for bipedal running," in *Humanoid Robots (Humanoids), 2010 10th IEEE-RAS International Conference on*, 2010, pp. 498–503.

[10] T. Tsuji, "A model of antagonistic triarticular muscle mechanism for lancelet robot," in *2010 11th IEEE International Workshop on Advanced Motion Control*. IEEE, Mar. 2010, pp. 496–501.

[11] V. Salvucci, Y. Kimura, S. Oh, and Y. Hori, "Force maximization of biarticularly actuated manipulators using infinity norm," *IEEE/ASME Transactions on Mechatronics*, vol. 18, no. 3, pp. 1080–1089, 2013.

[12] H. Fukusho, T. Sugimoto, and T. Koseki, "Control of a straight line motion for a two-link robot arm using coordinate transform of bi-articular simultaneous drive," in *Advanced Motion Control, 2010 11th IEEE International Workshop on*, 2010, pp. 786–791.

[13] T. Oshima, T. Fujikawa, O. Kameyama, and M. Kumamoto, "Robotic analyses of output force distribution developed by human limbs," in *Robot and Human Interactive Communication, 2000. RO-MAN 2000. Proceedings. 9th IEEE International Workshop on*, 2000, pp. 229–234.

[14] M. Kumamoto, T. Oshima, and T. Yamamoto, "Control properties induced by the existence of antagonistic pairs of bi-articular muscles – mechanical engineering model analyses," *Human Movement Science*, vol. 13, no. 5, pp. 611–634, Oct. 1994.

[15] V. Salvucci, Y. Kimura, S. Oh, and Y. Hori, "Experimental verification of infinity norm approach for force maximization of manipulators driven by bi-articular actuators," in *American Control Conference (ACC)*, 2011.

[16] V. Salvucci, Y. Kimura, S. Oh, T. Koseki, and Y. Hori, "Comparing approaches for actuator redundancy resolution in biarticularly-actuated robot arms," *IEEE/ASME Transactions on Mechatronics*, 2013.

[17] V. Salvucci, Y. Kimura, S. Oh, and Y. Hori, "Non-linear phase different control for precise output force of bi-articularly actuated manipulators," *Advanced Robotics*, pp. 1–12, Dec. 2012.

[18] ——, "BiWi: bi-articularly actuated and wire driven robot arm," in *2011 IEEE International Conference on Mechatronics*, 2011, pp. 827–832.

[19] S. Oh, V. Salvucci, and Y. Hori, "Development of simplified statics of robot manipulator and optimized muscle torque distribution based on the statics," in *American Control Conference (ACC), 2011*. IEEE, Jul. 2011, pp. 4099–4104.

[20] V. Salvucci, S. Oh, and Y. Hori, "Infinity norm approach for precise force control of manipulators driven by bi-articular actuators," in *IECON 2010 - 36th Annual Conference on IEEE Industrial Electronics Society*. IEEE, Nov. 2010, pp. 1908–1913.